A Computational Study of the Correlations between Structure and Dynamics in Free and Surface-Immobilized Single Polymer Chains

Jianyuan Shang and Eitan Geva*

Department of Chemistry, University of Michigan, Ann Arbor, Michigan 48109-1055

Received: May 2, 2005; In Final Form: July 6, 2005

The correlations between structure and dynamics in free and surface-immobilized polymers were investigated via Langevin dynamics simulations of a free-jointed homopolymer. A detailed analysis was performed for a polymer in free solution and a polymer attached to a surface. The cases of repulsive and attractive surfaces, as well as poor and good solvents, were considered. The analysis focuses on properties that are particularly relevant to single molecule measurements, namely: (1) the distribution of end-to-end distance, (2) the correlations between the conformational structure and the time scale of its motion, (3) the correlations, at equilibrium, between the end-to-end distance and its displacement, and (4) the correlation between the initial coil conformation and the collapse pathway into the globular state. The differences and similarities between this model and a previously considered model of a protein, with two-state folding kinetics and a well-defined native state, are also discussed.

I. Introduction

The elucidation of the structure and dynamics of polymers in solution has been the subject of many experimental, theoretical, and computational studies.[1,2] More recently, powerful single-molecule techniques have emerged which make it possible to study polymer structure and dynamics with an unprecedented level of detail.[3−41] In those experiments, one measures the variation over time of the efficiency of energy transfer between a donor dye molecule and an acceptor dye molecule, which label specific sites on the polymer. Those variations are then interpreted as reflecting the conformational dynamics of the polymer, since the efficiency of energy transfer is very sensitive to the donor−acceptor distance. More specifically, the rate constant for nonradiative fluorescence resonance energy transfer (FRET) from donor to acceptor is assumed to be given by the Förster theory, namely[45,47,48]

$$k_{\mathrm{ET}}(R) = k_{\mathrm{D}}\left(\frac{R_0}{R}\right)^6 \tag{1}$$

where, k_{D}^{-1} is the fluorescence lifetime of the free donor, R is the distance between donor and acceptor, and R_0 is a parameter that depends on the choice of the donor−acceptor pair and other experimental conditions.[49]

Single-molecule FRET experiments are typically performed by using a dual-channel detection scheme. More specifically, one photoexcites the donor with continuous wave (CW) radiation, while simultaneously detecting the fluorescence photons from the donor *and* the acceptor in a selective manner. The fraction of photons detected in the acceptor channel, over a given time-averaging window of length T_W, provides a direct measure of the time-averaged FRET efficiency, which we will denote by $E_{\mathrm{ET}}(T_W)$. One may then *define* a time-averaged and T_W-dependent donor−acceptor distance, which will be denoted by $\langle R\rangle_{TW}$, such that

$$E_{\mathrm{ET}}(T_W) \equiv \frac{1}{1 + [\langle R\rangle_{TW}/R_0]^6} \tag{2}$$

The requirement that T_W is sufficiently long to establish $E_{\mathrm{ET}}(T_W)$ with a reasonable signal-to-noise ratio is often difficult to satisfy in free solution, where T_W is dictated by the time that the molecule spends in the focal volume. Hence, it is often necessary to spatially confine the polymer in order to minimize the shot noise. One way of achieving this is by attaching the polymer to a surface. However, this popular practice also raises important questions regarding the impact of surface immobilization on the polymer's structural and dynamical properties.

The actual value of T_W also dictates the type of information that can be extracted from single-molecule FRET experiments. If T_W is very short in comparison to the time scale on which R changes, then R remains fixed during the measurement and $E_{\mathrm{ET}}(T_W) = \{1 + [R/R_0]^6\}^{-1}$, where R is the instantaneous R. In such a case, there is a direct and exact relationship between the probability distributions of E_{ET} and R

$$P(R) = P(E_{\mathrm{ET}} = (1 + [R/R_0]^6)^{-1})\,\frac{\mathrm{d}}{\mathrm{d}R}(1 + [R/R_0]^6)^{-1} \tag{3}$$

On the other hand, if T_W is longer than the time scale on which R changes, then $E_{\mathrm{ET}}(T_W)$ will coincide with its ensemble average, $\bar{E}_{\mathrm{ET}}$, and have the same value regardless of which time window it was measured on. In practice, one is usually between those two limits, such that there is a distribution of values of $E_{\mathrm{ET}}(T_W)$, which is narrower than in the limit $T_W \rightarrow 0$ but does not have a zero width, as in the limit $T_W \rightarrow \infty$.

A unique feature of single-molecule FRET experiments has to do with their ability to provide *dynamical* information. Such dynamical information has been extracted in several ways. Jia et al. have monitored $P(\langle R\rangle_{T_W})$ (the distribution of $\langle R\rangle_{T_W}$) as a function of T_W, in the case of a surface-immobilized polypeptide, and found that conformations corresponding to smaller values of $\langle R\rangle_{T_W}$, move on a faster time scale.[11] Talaga et al.[23] have considered the correlation between the square displacement of the donor−acceptor distance (divided by T_W)

$$D(j) = [\langle R\rangle_{T_W}(j+1) - \langle R\rangle_{T_W}(j)]^2/T_W \tag{4}$$

10.1021/jp052275c CCC: $30.25
Published on Web 08/06/2005

and the value of $\langle R\rangle_{T_w}(j)$. Here, $\langle R\rangle_{T_w}(j)$ and $\langle R\rangle_{T_w}(j+1)$ correspond to the averaged value of R on the subsequent j and $(j+1)$th time windows. Rhoades et al.[32] have performed single-molecule FRET measurements on proteins trapped within surface-tethered lipid vesicles and reported a wide and structured distribution of $\Delta R(j) = \langle R\rangle_{T_w}(j+1) - \langle R\rangle_{T_w}(j)$, with preference to relatively small values. These observations were attributed to the heterogeneous and multistep nature of the protein folding/unfolding process.

Single-molecule FRET experiments provide direct information on the distributions of structural parameters such as the end-to-end distance, as well as their correlation to the dynamics of conformational fluctuations. Other single-molecule techniques, such as force-clamp atomic force microscopy,[18] also provide powerful experimental probes into the conformational dynamics of polymers. For example, such an approach can allow for the measurement of correlations between the initial coiled, or unfolded, conformation and the rate of its collapse into a globular, or folded, conformation.

The interpretation of single-molecule experiments in polymers and biopolymers has been the subject of several recent theoretical and computational studies.[34−41] Bagchi and co-workers have used Brownian dynamics simulations to investigate the distribution of the FRET efficiency at equilibrium and during the collapse of a freely jointed homopolymer,[38,41] the dependence of the end-to-end distance distribution on the stiffness of the polymer,[40] and the FRET survival probability within the context of the Rouse chain model.[39] Yang and Cao have derived analytical expressions for the end-to-end distance distribution, as well as the correlation between the end-to-end distance and its displacement, in the case of a semiflexible Gaussian chain model.[34] Gopich and Szabo have presented a theoretical analysis of how the end-to-end distance distribution, and the potential of mean force derived from it, depend on the time-averaging window.[35] Those authors have also used their theory to demonstrate the effect of time averaging in the cases of a Gaussian chain model and a kinetic model for protein folding on a reduced 2D free energy surface.[35]

In a previous paper, we employed Langevin dynamics simulations of a polypeptide chain to explore the ability of single-molecule FRET experiments to provide new information on the structure and dynamics of biopolymers.[36] The polypeptide model employed consisted of a relatively short single-chain heteropolymer that consists of 22 beads, and the sequence along the backbone was chosen to dictate a unique native state and two-state kinetics. The analysis was also limited to the case of a polypeptide in free solution. In the present paper, we present the results of a similar analysis in the case of a significantly longer (128 beads) free-jointed homopolymer model, whose state changes as a function of the solvent quality, from coiled (in a good solvent) to globular (in a poor solvent). Emphasis is put on the structural and dynamical effects due to immobilization on attractive and repulsive surfaces and the correlation between the structure of the initial coiled conformation and the rate of its nonequilibrium collapse into the globular state. The discussion focuses on quantities which are relevant to single-molecule FRET experiments and aims at elucidating the unique ability of those experiments to provide information on the correlations between structure and conformational dynamics. Special attention is also given to understanding the similarities and differences between the homopolymer model and the protein model of ref 36, from the point of view of those FRET-related quantities.

The plan of this paper is as follows. In section II, we provide a short overview of the model and simulation techniques. In section III, we report the results obtained for the equilibrium distributions of the radius of gyration and end-to-end distance, equilibrium correlation functions of the end-to-end distance, correlations between the end-to-end distance and its displacement, and correlations between the initial coil conformation and its collapse rate and pathway. A summary of the results and a discussion of their relationship to other studies is provided in section IV.

II. Model and Simulation Techniques

The analysis in the following section is based on results obtained from Langevin dynamics simulations performed on a freely jointed single-chain homopolymer that consists of $N = 128$ identical beads. The intramolecular potential energy of the homopolymer is given by

$$V = V_{\mathrm{BL}} + V_{\mathrm{NB}} \tag{5}$$

where V_{BL} and V_{NB} correspond to the bond-length potential and nonbonding interactions, respectively. V_{BL} is given by

$$V_{\mathrm{BL}} = \sum_{k=1}^{N-1} \upsilon_{\mathrm{BL}}(r_{k,k+1}) \tag{6}$$

where $r_{i,j}$ is the distance between the ith and jth beads and imposes connectivity along the chain, via a spring potential of the form $\upsilon_{\mathrm{BL}}(r) = {}^1/_2 k(r-a)^2$. The nonbonding interaction term is given by

$$V_{\mathrm{NB}} = \sum_{k=1}^{N-1} \sum_{l=k+1}^{N} \upsilon_{\mathrm{NB}}(r_{k,l}) \tag{7}$$

where

$$\upsilon_{\mathrm{NB}}(r) = 4\epsilon\left[\left(\frac{\sigma}{r}\right)^{12} - \lambda\left(\frac{\sigma}{r}\right)^{6}\right] \tag{8}$$

The parameter λ determines the quality of the solvent, such that $\lambda = 0$ in a good solvent and $\lambda = 1$ in a poor solvent.

The polymer dynamics is modeled within the framework of the Langevin equation

$$m\frac{\mathrm{d}^2\vec{r}_j}{\mathrm{d}t^2} = -\zeta\frac{\mathrm{d}\vec{r}_j}{\mathrm{d}t} - \vec{\nabla}_j V + \vec{\Gamma}_j \tag{9}$$

Here, m is the mass of a bead, $\vec{r}_j$ is the position of the jth bead ($j = 1, ..., N$), $-\vec{\nabla}_j V$ and $\vec{\Gamma}_j$ are the systematic and random forces it is subject to, respectively, and ζ is the friction coefficient. Equation 9 was integrated numerically via the Verlet algorithm.[50,51] Temperature is introduced via the variance of the Gaussian random force, which is assumed to be δ-correlated.

Simulations were performed in the cases of a free polymer or a polymer immobilized on a surface. The surface was assumed to be planar and to consist of beads of diameter a that were arranged on a 2D cubical lattice with distance a between the centers of mass of nearest neighbors. Surface immobilization was introduced by fixing the position of the 64th bead such that it lies on top of one of the surface beads, with a distance a between the corresponding centers of mass. Two generic types of interactions between the polymer and the surface beads were considered. In one case, we assumed that the interactions between the polymer and the surface beads are repulsive and

described by $v_{NB}(r)$ with $\lambda = 0$. In the second case, we assumed that the interactions between the polymer and the surface beads are attractive and described by $v_{NB}(r)$ with $\lambda = 1$ (cf. eq 8).

The simulation results are presented below in terms of reduced units. More specifically, the units of mass, energy, length, and time are given by m, ϵ, a, and $\sqrt{ma^2/\epsilon}$, respectively. The following values of the parameters were employed in the simulations reported below: $k_BT = 0.40$, $k = 100.0$, $\sigma = 1.0$, and $\zeta = 0.05$. The integration time step was given by $\delta t = 0.005$.

Equilibrium properties were obtained by averaging over 10 trajectories in the case of the free polymer and a polymer on a repulsive surface and 20 trajectories in the case of a polymer on an attractive surface (because of the slower time scale of the dynamics in the latter). Each trajectory starts with an equilibration period of 10^5-10^6 time steps, followed by a data collection period of 5.0×10^6 time steps. Nonequilibrium simulations of the polymer collapse start with a randomly chosen and equilibrated coiled conformation, followed by an abrupt change in the solvent quality from "good" to "poor" (see section III. D for more details).

III. Results

A. Typical Conformations and Equilibrium Distributions of the Radius of Gyration and the End-to-End Distance. We will start the discussion of the results with a qualitative description of the types of conformations that dominate under different conditions. We first consider the case of a free polymer. As is well-known, a good solvent will give rise to coiled conformations, while a poor solvent will give rise to more compact globular conformations. Typical conformations, as obtained from our free polymer simulations, for the model considered here, are shown in Figure 1a (globule) and Figure 1b (coil). It should be noted that the arrangement of the polymer beads in the globular conformation is liquid-droplet-like. A qualitatively similar picture is also obtained from simulations where the polymer is immobilized on a repulsive surface (see Figure 1c,d). In this case, the interaction of the polymer beads with the surface are of the excluded volume type and have a relatively small impact on the structure of the conformations in either poor of good solvents.

Immobilization on an attractive surface gives rise to a qualitatively different picture. In the case of a good solvent, one observes a strong tendency for forming conformations where many of the polymer beads are in the close vicinity (i.e., within a distance of σ or so) of the surface (see Figure 1f). This observation is to be expected in the case of a sticky surface and suggests a shift from conformations typical of a random coil in 3D to those expected from a random coil in 2D. The conformations observed for an immobilized polymer on an attractive surface in the case of a poor solvent are also rather different than in the cases of a free polymer and a polymer immobilized on a repulsive surface. A typical "globular" conformation consists of several layers, which are parallel to the surface and are separated by a distance of about σ (see Figure 1e). The number of beads in each layer decreases, on average, with increasing distance from the surface. Those structures should be contrasted with the isotropic liquid-droplet-like configurations observed in the cases of a free polymer and a polymer immobilized on a repulsive surface.

A more quantitative perspective of the conformations expected under different conditions can be obtained by considering the equilibrium distributions of the radius of gyration

$$R_G = \frac{1}{N}\sqrt{\frac{1}{2}\sum_{k,l=1}^{N} r_{k,l}^{\,2}} \tag{10}$$

and end-to-end distance, $R = r_{1,N}$. Those distributions, as obtained from simulations performed under different conditions, are shown in Figures 2 and 3, respectively. It should be noted that calculating those distributions in the case of a polymer on an attractive surface required about twice as much averaging (in the presence of either good or poor solvents), which is indicative of slower dynamics (a more detailed discussion of dynamical aspects is provided in the following sections). Also shown in Figure 3 are the potentials of mean force. The latter is given by $V_{mf}(R) = -k_BT \ln[P_{eq}(R)]$, where $P_{eq}(R)$ is the equilibrium distribution of the end-to-end distance.

In the presence of a good solvent, the R_G distribution on the attractive surface is wider and shifted to longer R_G relative to the free polymer. The opposite trend is observed in the case of a repulsive surface, where the distribution is somewhat narrower and shifted to smaller R_G relative to the free polymer (cf. Figure 2). The tendency of the repulsive surface to decrease the size of the polymer can be attributed to the exclusion of stretched conformations where the two arms of the polymer chain would be lying on opposite sides of the surface. The tendency of the attractive surface to increase the size of the polymer can be attributed to the transition from a 3D to a 2D space of conformations (see below).

In the presence of a poor solvent, very similar R_G distributions are obtained for a free polymer and a polymer on a repulsive surface. However, the R_G distribution on an attractive surface is significantly different in this case. More specifically, it is wider and centered around a higher value of R_G, which is a signature of the flattened structure of the globular conformations, as depicted in Figure 1e.

The distributions of the end-to-end distance, R, in the case of a good solvent, show similar trends to the corresponding radius of gyration distributions (cf. Figures 2 and 3). More specifically, the R distributions become wider and shift to larger values of R as we move from a polymer on a repulsive surface, through the case of a free polymer, to a polymer on an attractive surface. Interestingly, in the case of ideal chains with an exclusive volume effect, one expects a Gaussian distribution of R, with an average that satisfies the following scaling law:[1]

$$\langle R \rangle = N^{\upsilon} \tag{11}$$

where $\upsilon = {}^3/_4$ and ${}^3/_5$ in 2D and 3D, respectively. For $N = 128$, this yields $\langle R \rangle = 35$ and 18 in 2D and 3D, respectively. The distributions in Figure 3 are indeed Gaussian-like, with averages at $\langle R \rangle = 36$, 22, and 20 on the attractive surface, in free solution, and on a repulsive surface, respectively. This trend is indicative of the expected transition from a 3D to a 2D space of conformations, as is also suggested by Figure 1b,d,f.

In the case of a poor solvent, the R distributions are rather different from the corresponding R_G distributions (cf. Figures 2 and 3). More specifically, the R distributions have a similar width in all three cases, but differ in structure. The R distributions are similar in the cases of a free polymer and a polymer on a repulsive surface, where the structure is indicative of liquidlike spherical solvation shells. The R distribution for a polymer on an attractive surface is distinctly different. More specifically, the prominent first peak in this distribution corresponds to the distance between subsequent layers in what are distinctly different globular conformations (cf. Figure 1e). It should be noted that the peaks at higher values of R are rather

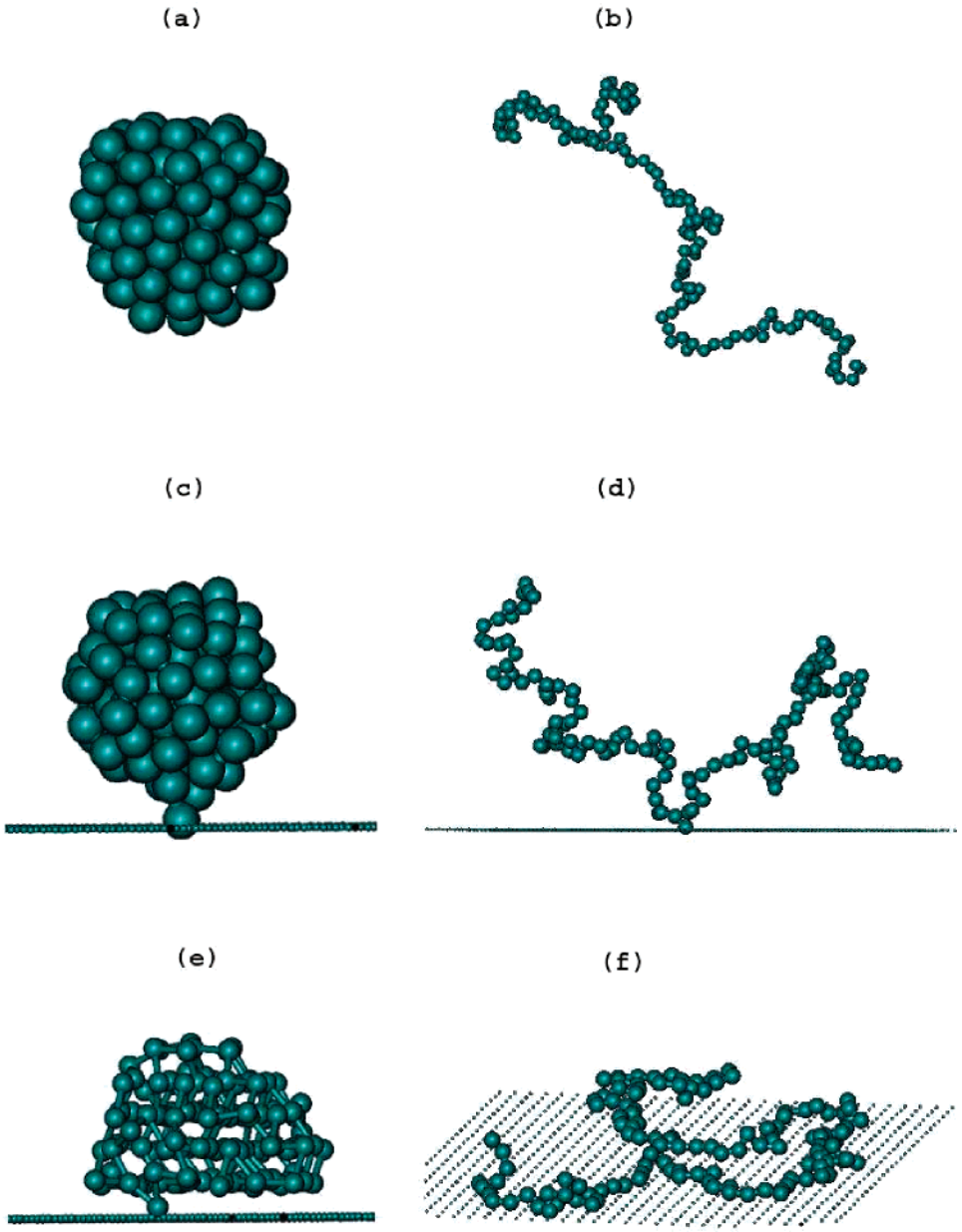

Figure 1. Typical conformations under different conditions: (a) free polymer in a poor solvent; (b) free polymer in a good solvent; (c) polymer on a repulsive surface in a poor solvent; (d) polymer on a repulsive surface in a good solvent; (e) polymer on an attractive surface in a poor solvent; (f) polymer on an attractive surface in a good solvent.

similar to those obtained in the case of a free polymer and a polymer on a repulsive surface, which can be attributed to the fact that the globular structure acquires a more liquidlike nature on a longer length scale.

It should be noted that the R distributions reported here correspond to $P(\langle R\rangle_{T_W})$ when $T_W \rightarrow \delta t$. We have also calculated $P(\langle R\rangle_{T_W})$ at longer values of T_W (not shown). Increasing T_W was observed to uniformly narrow the distribution in the case of a good solvent, which implies that the time scale of conformational dynamics was relatively insensitive to the value of R, i.e., to the specific structure of the coiled conformation. This should be contrasted with the protein model analyzed in ref 36, where a nonuniform narrowing of the R distribution was observed in the unfolded state, which implied that conformations with short R values move on a faster time scale. In the case of a poor solvent, we have found $P(\langle R\rangle_{T_W})$ to be relatively insensitive to the changes of T_W within the range accessible by our simulations. This should also be contrasted with the protein model of ref 36, where the very rapid dynamics in the folded state has led to significant narrowing of $P(\langle R\rangle_{T_W})$ with increasing T_W.

B. Equilibrium Time Correlation Functions of the End-to-End Distance. Some insight into the characteristic time scales of conformational dynamics can be obtained from the corresponding equilibrium correlation functions of the end-to-end distance, R

$$C(t) = \frac{\langle R(t)R\rangle - \langle R\rangle^2}{\langle R^2\rangle - \langle R\rangle^2} \tag{12}$$

We have calculated this correlation function for a free polymer and polymers immobilized on repulsive and attractive surfaces, in good and poor solvents. The results are presented in Figure 4 on a semilog plot.

The decay of $C(t)$ is seen to stretch over a relatively wide range of time scales in all of the cases considered. In the case

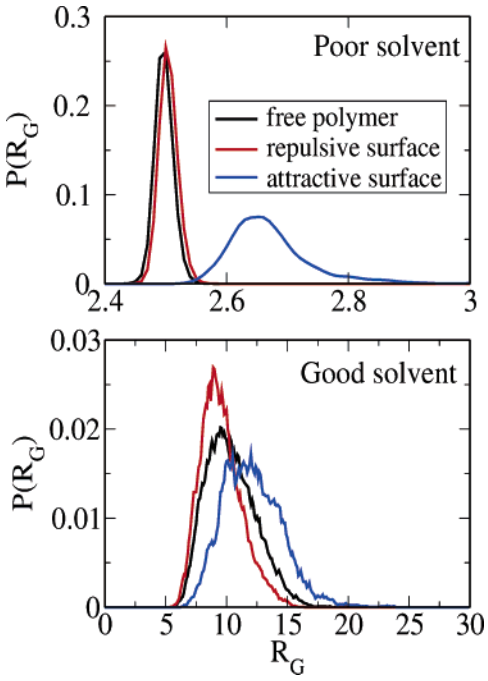

Figure 2. Distributions of the radius of gyration in a poor solvent (top) and a good solvent (bottom).

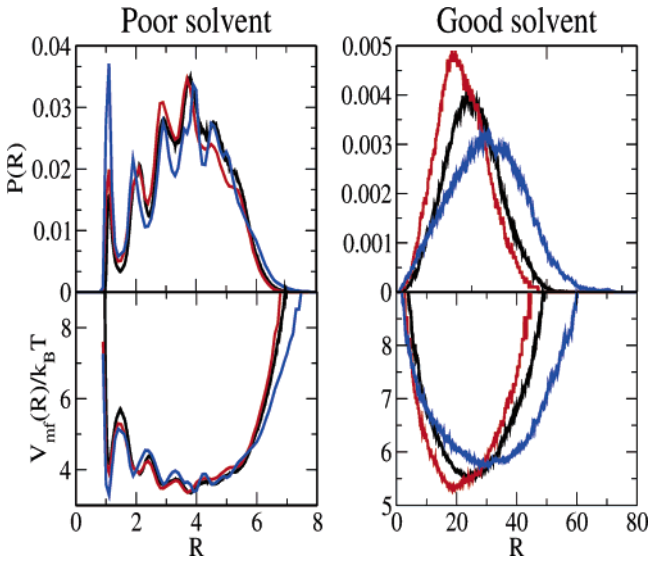

Figure 3. Distributions of the end-to-end distance in a poor solvent (left) and a good solvent (right). Also shown are the corresponding potentials of mean force (bottom). Red, black, and blue correspond to a polymer immobilized on a repulsive surface, a free polymer, and a polymer immobilized on an attractive surface, respectively.

of a free polymer, we find that $C(t)$ stretches over a longer range of time scales in a poor solvent. This trend can be attributed to the rough potential of mean force in a poor solvent, which should be contrasted with the smooth potential of mean force in a good solvent (cf. Figure 3). The contributions at longer time scales in a poor solvent can be attributed to relatively slow barrier crossing processes, which correspond to the motion of beads between the liquidlike shells of the globular conformations. The contributions at shorter times can be attributed to intrashell oscillations, which are characterized by relatively short periods. It is interesting to contrast this trend with that observed in the case of the protein model of ref 36, where the dynamics of the folded conformation has been observed to occur on time scales which are faster in comparison to unfolded conformations.

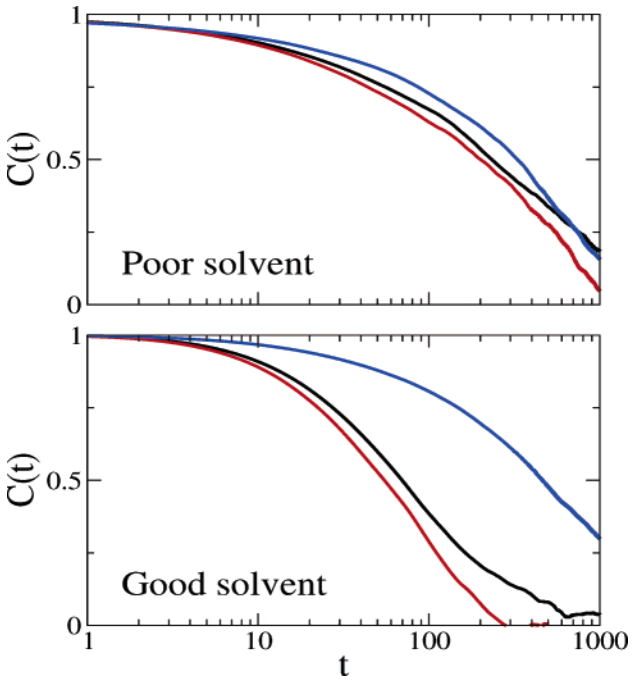

Figure 4. Time correlation functions of the end-to-end distance in poor (top panel) and good (bottom panel) solvents. Red, black, and blue correspond to a polymer immobilized on a repulsive surface, a free polymer, and a polymer immobilized on an attractive surface, respectively.

This behavior in proteins can be attributed to the fact that the potential of mean force for the folded conformation corresponds to a *single* very deep and rather narrow well, which is centered around the native state. At the same time, the globular confirmations of the polymer are liquidlike, with a potential of mean force that is characterized by multiple minima.

In the case of a polymer on a repulsive surface, we also find that the correlation function in a good solvent stretches to longer and shorter time scales than in a poor solvent. In fact, the dynamical time scales are very similar to those observed in the case of a free polymer. Thus, in this case, the surface has a minimal impact on both structure and dynamics of the conformations. The situation is rather different in the case of a polymer on an attractive surface. More specifically, $C(t)$ shows similar behaviors in the presence of good and poor solvents. and particularly so at long times. The relatively slow time scale in the case of a poor solvent is attributed to the relatively slow barrier crossing dynamics which is associated with rearrangements of the layered structure in the globular state. The relatively slow dynamics in the case of a good solvent is associated with the relatively large barriers that need to be crossed when detaching segments of the polymer from the surface, which is necessary for rearranging the conformation. Because the bead−bead and bead−surface interactions are identical in this case, one expects similar barriers in both cases, and hence similar times scales.

C. Correlation between Structure and Dynamics at Equilibrium. We next consider the correlation between structure and dynamics at equilibrium.[36] To this end, we divide the overall simulation time into the time windows of length T_W and define $\langle R\rangle_{T_W}(j)$ as the averaged value of R over the jth time window. If T_W is very short in comparison to the time scale on which R changes, then $\langle R\rangle_{T_W}(j)$ is equal to the instantaneous value of R. On the other hand, if T_W is longer than the time scale on which R changes, then $\langle R\rangle_{T_W}(j)$ will coincide with its ensemble average

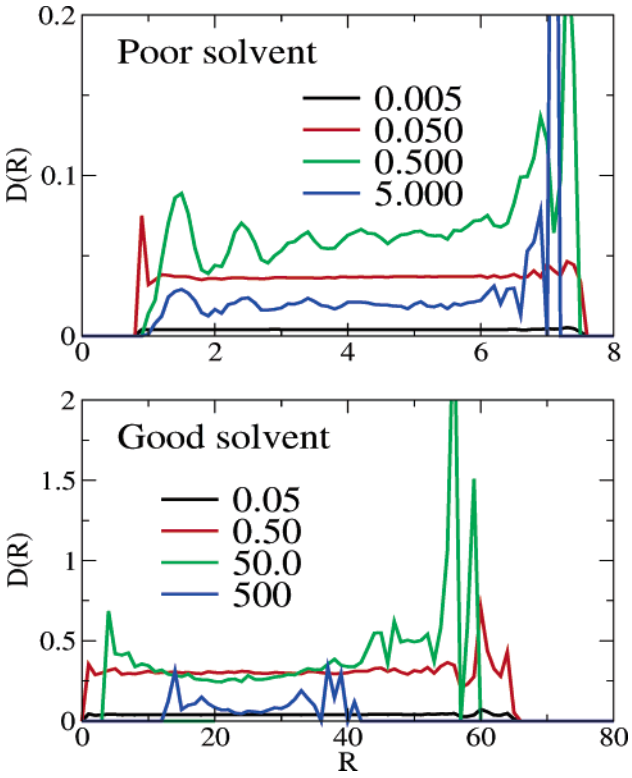

Figure 5. The dependence of $\bar{D}(\langle R\rangle_{T_W})$ on $\langle R\rangle_{T_W}$ for a free polymer in a poor solvent (top) and in a good solvent (bottom). The results are reported for the indicated values of the averaging time window, T_W. The numerical noise at short and long distances is due to their relative rarity, which leads to increasingly poor statistics.

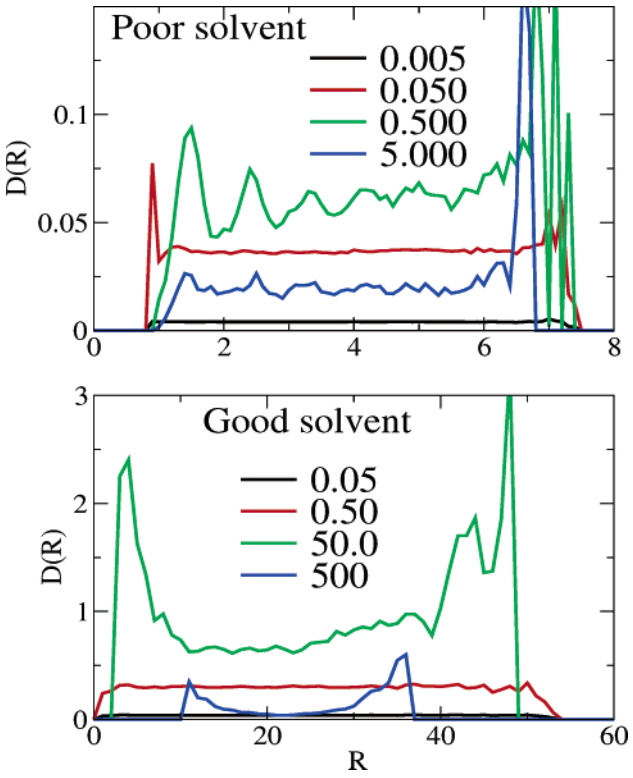

Figure 6. Same as Figure 5 for a polymer on a repulsive surface.

and has the same value regardless of which time window it was measured on.

A related useful quantity is given by $D(j)$ and corresponds to the square displacement of $\langle R\rangle_{T_W}$, divided by T_W, as defined in eq 4. It should be noted that the probability distribution of R, and the corresponding instantaneous velocity, $\dot{R}$, are uncorrelated ($P(R,\dot{R}) \propto \exp[-V_{mf}(R)/k_BT] \times \exp[-m\dot{R}^2/2k_BT]$). Thus, for a very short time window, $T_W = \delta t$, the average value of $D(j)$, over the subset of conformations that correspond to the same end-to-end distance, R, will be constant and *independent* of R: $\bar{D}(R) = \overline{\dot{R}^2}\delta t = k_BT\delta t/m$. It should also be noted that, in this case, $\bar{D}(R)$ becomes vanishingly small for a truly infinitesimal δt (in practice, δt corresponds to the simulation time step, which is chosen to be much shorter than the fastest dynamical time scale in the model under consideration). The opposite extreme corresponds to the case where T_W is very large in comparison to the characteristic time scale of conformational dynamics. In this case, the ergodic hypothesis implies that averaging R over the time window is equivalent to taking the ensemble average, namely $\langle R\rangle_{T_W} = \bar{R}$. The value of D will vanish at that single value of $\langle R\rangle_{T_W}$, since $\langle R\rangle_{T_W}(j+1) = \langle R\rangle_{T_W}(j) = \bar{R}$. Thus, no information regarding correlations between structure and dynamics can be obtained in the extreme limits of very short or very long averaging time windows. However, such information can still be obtained if one chooses an intermediate averaging time window, which is comparable to the relevant time scale of the conformational dynamics. The fact that D is nonnegative and vanishes at the limits $T_W \to 0$ and $T_W \to \infty$ also implies that the dependence of $\bar{D}(\langle R\rangle_{T_W})$ on T_W is nonmonotonic and will exhibit a turnover.

The dependence of $\bar{D}(\langle R\rangle_{T_W})$ on $\langle R\rangle_{T_W}$, as obtained from the simulations of a free polymer, is presented in Figure 5 in the cases of good and poor solvents. The dependence is shown in those figures for different averaging time windows. In a poor solvent (top panel in Figure 5), $\bar{D}(\langle R\rangle_{T_W})$ is observed to go through a turnover as a function of T_W. As expected, $\bar{D}(\langle R\rangle_{T_W})$ becomes very small and is not correlated with $\langle R\rangle_{T_W}$ at the smallest time window ($T_W = \delta t = 0.005$). This lack of correlation persists when T_W is increased, until it becomes comparable to the time scale of intrashell oscillations ($T_W = 0.50$). At this point, $\bar{D}(\langle R\rangle_{T_W})$ develops structure. Furthermore, the structure is reminiscent of that of the end-to-end distance distribution and potential of mean force for the same case (cf. Figure 3). The fact that the minima in $\bar{D}(\langle R\rangle_{T_W})$ correspond to the minima in the potential of mean force is consistent with the expectation that the characteristic time scale for intrashell dynamics is *faster* than that of intershell, barrier-crossing, dynamics. Further increasing the time window leads to an overall decrease in $\bar{D}(\langle R\rangle_{T_W})$ and smearing of the structure, as the averaging time window becomes comparable to or larger than the time scale of shell rearrangements.

In a good solvent (bottom panel in Figure 5), $\bar{D}(\langle R\rangle_{T_W})$ is also observed to go through a turnover as a function of T_W. A nontrivial correlation between $\bar{D}(\langle R\rangle_{T_W})$ and $\langle R\rangle_{T_W}$ emerges at values of T_W which are significantly higher than those in a poor solvent ($T_W = 50.0$). This can be attributed to the narrower dynamical range in this case (cf. Figure 4). It should also be noted that the dependence of $\bar{D}(\langle R\rangle_{T_W})$ on $\langle R\rangle_{T_W}$ in this region follows a relatively smooth curve, which is consistent with the potential of mean force in the coiled state (cf. Figure 3).

The dependence of $\bar{D}(\langle R\rangle_{T_W})$ on $\langle R\rangle_{T_W}$, as obtained from the simulations of a polymer attached to repulsive and attractive surfaces, are presented in Figures 6 and 7, respectively, in the cases of good and poor solvents. As for the distribution of the end-to-end distance, the results in the case of the repulsive surface are very similar to those obtained in the case of a free polymer. The results in the case of the attractive surface are also rather similar and indicate that the dynamics are rather

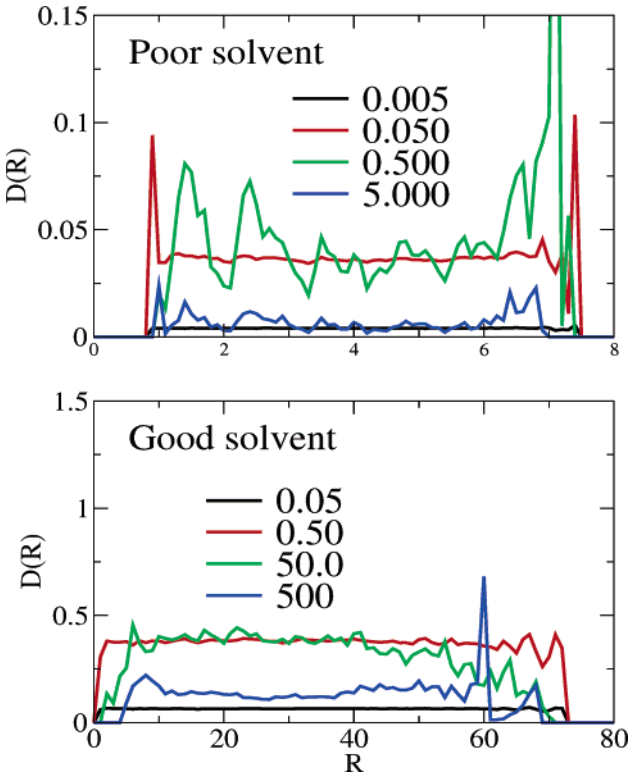

Figure 7. Same as Figure 5 for a polymer on an attractive surface.

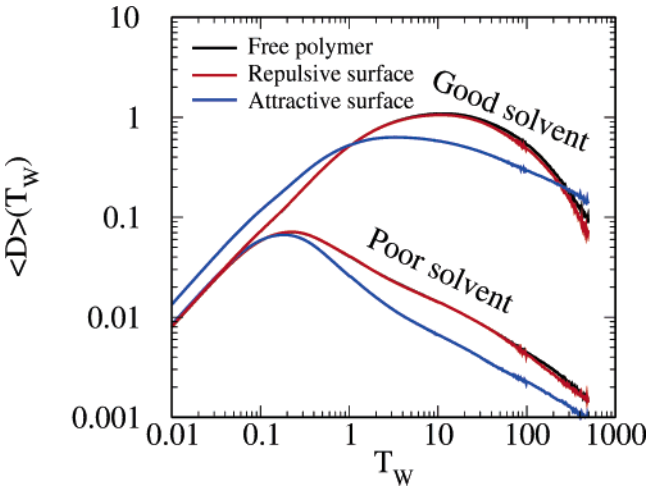

Figure 8. The average value of $\bar{D}(\langle R\rangle_{T_W})$ as a function of T_W under different conditions. Red, black, and blue correspond to a polymer immobilized on a repulsive surface, a free polymer, and a polymer immobilized on an attractive surface, respectively.

similar despite the fact that the conformations in this case are structurally rather different from those in the free polymer and a polymer immobilized on a repulsive surface. This is to be expected since the bead−surface and bead−bead interactions in the attractive surface case are the same as the bead−bead interactions in the cases of a free polymer and a polymer on a repulsive surface.

Finally, we consider the average value of $\bar{D}(\langle R\rangle_{T_W})$, as a function of T_W, under different conditions. The results are shown in Figure 8. As expected, the results in the cases of a free polymer and a polymer on a repulsive surface are almost indistinguishable. In all cases, one also observes the expected turnover behavior. It should be noted that correlations between structure and dynamics in Figures 5, 6, and 7 are observed at values of T_W which correspond to the vicinity of the peak in the turnover curve. It should also be noted that the turnover occurs at shorter T_W in the case of a poor solvent. This reflects the fast intrashell (in the case of a free polymer or a polymer on a repulsive surface) or intralayer (in the case of the attractive surface) dynamics. It should be noted that the slower intershell or interlayer dynamics do not affect the average value of $\bar{D}(\langle R\rangle_{T_W})$. This is because motion between the minima on the potential of mean force is relatively rare, such that $\langle R\rangle_{T_W}(j)$ and $\langle R\rangle_{T_W}(j+1)$ mostly reflect averaging over the faster intrashell or intralayer dynamics *within the same shell or the same layer*.

D. Correlation between the Initial Coil Conformation and the Collapse Rate. In this section, we consider the collapse process from a coiled conformation into a globule. To this end, we performed simulations that start with randomly chosen coil conformations from an ensemble that was obtained by equilibrating the polymer subject to the constraint $R = R_0$ (introduced by a harmonic potential of the form $k(R - R_0)^2/2$), in a good solvent. This was followed by abruptly substituting the good solvent by a poor one and following the subsequent collapse into a globular conformation. Initial end-to-end distances ranging between 5.0 and 40.0, in increments of 1.0, were considered (this range is consistent with the distributions shown in Figure 3). A total of 100 independent collapse trajectories were simulated for each initial end-to-end distance.

The collapse rate for a given initial end-to-end distance was defined by the average of the inverse first passage time over the 100 collapse trajectories

$$k_c(R) = \frac{1}{N_t}\sum_{n=1}^{N_t}\frac{1}{\tau_n} \qquad (13)$$

where the sum is over the $N_t = 100$ trajectories that all start at a randomly picked initial coil confirmation with the same end-to-end distance, R, and τ_n is the first passage time for the nth trajectory. The first passage time was defined as the time it takes for R_G^2 to becomes smaller than 6.5, which is characteristic of the globular state. It should be noted that the range $R_G^2 < 6.5$ is well-separated from that in the coiled state, where $30.0 < R_G^2 < 395$ (cf. Figure 2). We have also used this data set in order to generate the dependence of the collapse rate on the radius of gyration of the initial coiled conformation.

The dependences of the collapse rate on the initial end-to-end distance and radius of gyration are shown in Figure 9 for the cases of a free polymer and a polymer on a repulsive surface. The results in both cases are rather similar, which implies that, as in the case of equilibrium fluctuations, immobilization on a repulsive surface has little impact on the nonequilibrium collapse process. The results demonstrate the expected trend of a decreasing collapse rate with increasing end-to-end distance and radius of gyration. We have also explored the relationship between the initial coiled conformation and the collapse pathway. On the basis of the simulation results, we could distinguish between two types of collapse pathways. In one type, the collapse proceeded in two steps, starting with the formation of local blobs separated by linear segments, which later coalesce into a globule. In the second type, the polymer goes through a smooth transition from the initial coiled conformation into the globular conformation, without discernible intermediate steps. Examples for those two types of collapse pathways are shown in Figure 10. On the basis of the simulation results, we have also observed a clear correlation between the initial end-to-end distance and the collapse pathway. More specifically, the two-step pathway is seen to be favored by initial coiled conforma-

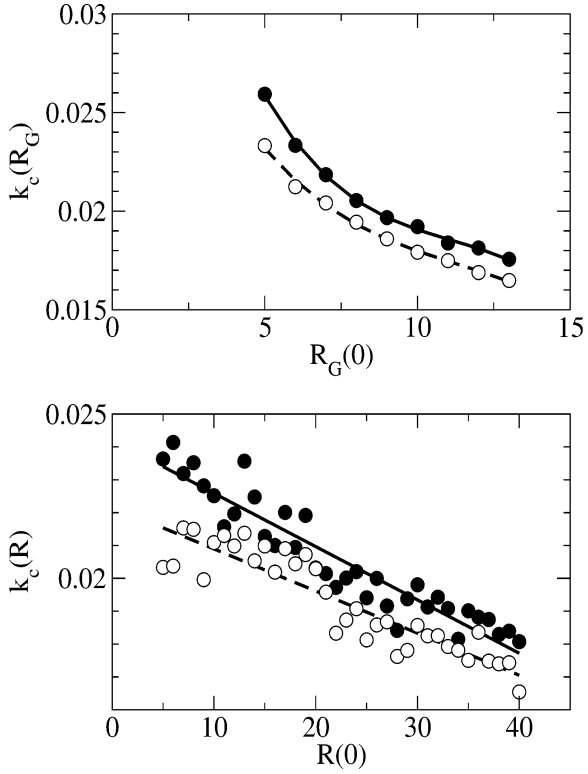

Figure 9. The dependence of the collapse rate on the radius of gyration (top panel) and end-to-end distance (bottom panel) of the initial coiled conformation, for a free polymer (solid line, black symbols) and a polymer immobilized on a repulsive surface (dashed line, white symbols). The guiding lines were obtained by the best fit to a cubical (top) and linear (bottom) polynomials.

tions with large end-to-end distances. For example, in the case where $R = 5.0$ in the initial conformation, about 15−20% of the trajectories followed the two-step pathway, while in the case where $R = 40.0$ in the initial conformation, 40−60% of the trajectories followed this pathway. This trend can probably be attributed to the fact that collapse by coalescing disconnected nearby segments provides a more efficient mechanism for collapse, except for cases where the initial conformation is relatively stretched, such that "blobbing" along the polymer backbone becomes the only available pathway for collapse. We have also attempted to simulate the collapse from a coil into a globule in the case of a polymer attached to an attractive surface. However, we were unable to obtained satisfactory statistics for the correlations between the initial conformation and the collapse rate, because of the exceedingly slow collapse rates observed in this case. In an effort to better understand the slowdown in the collapse rate, we have examined the dependence of the average collapse rate on the surface "attractiveness". To this end, we computed average collapse rates at different values of λ, ranging from $\lambda = 0$ (repulsive) to $\lambda = 1$ (attractive), by averaging over 100 trajectories with randomly chosen initial coiled conformations. It should be noted that a λ-dependent range of R_G^2 for the collapsed state was used in order to define the first passage time. The results are shown in Figure 11 and show a sharp slowdown in the collapse rate starting at around $\lambda = 0.70$. The onset of the slowdown suggests a sharp transition from conformational dynamics in 3D and liquidlike globular conformations at $\lambda < 0.7$ into conformational dynamics in 2D and layered globular conformations at $\lambda > 0.7$. A more detailed analysis of this interesting behavior will be the subject of future research.

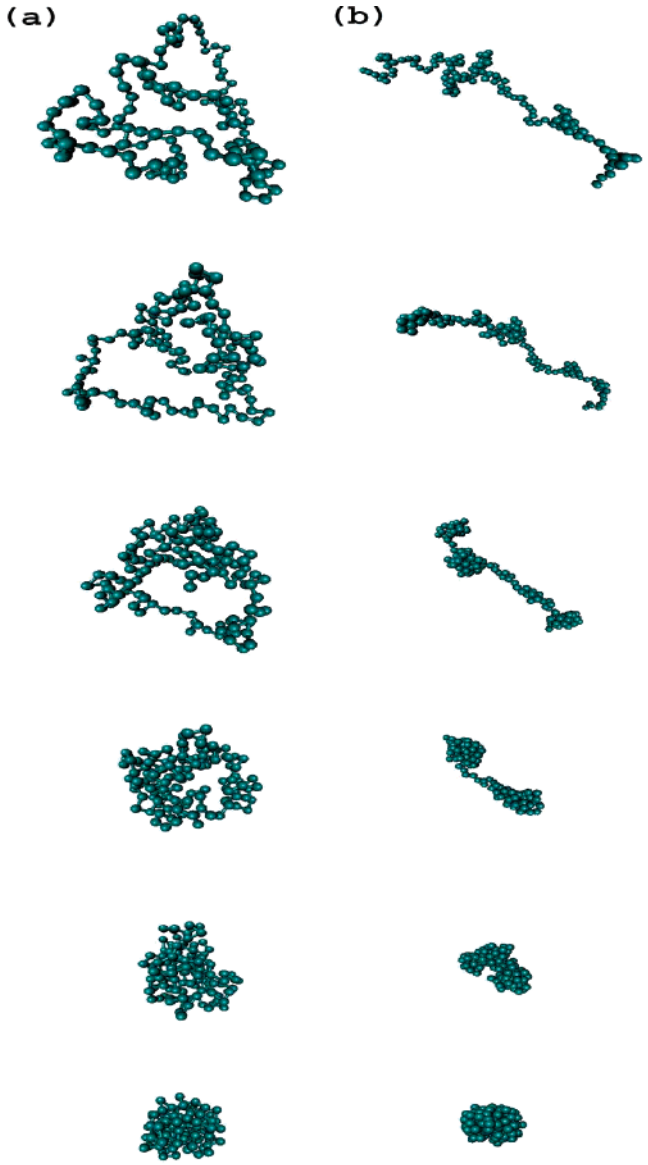

Figure 10. The two types of collapse pathways. In the collapse described in panel (a), the initial conformation is characterized by a short end-to-end distance and a small radius of gyration. Its collapse pathway goes through a smooth transition from the initial coiled conformation into the globular conformation, without discernible intermediate steps. In the collapse described in panel (b), the initial conformation is characterized by a long end-to-end distance and a large radius of gyration. Its collapse proceeds in two steps, starting with the formation of local blobs separated by linear segments, which later coalesce into a globule.

IV. Concluding Remarks

Experimental single-molecule techniques provide a unique opportunity for exploring the relationship between structure and dynamics in polymers. In this paper, we considered quantities which are relevant for those types of experiments by using Langevin dynamics simulations of a relatively long free-jointed homopolymer model. The analysis gives rise to several nontrivial predictions that can be tested experimentally. Particularly interesting predictions pertain to the impact of surface immobilization on the end-to-end distance distributions, the correlations between the end-to-end-distance and its displacement, and the collapse rate, as well as the correlation between the latter and initial coiled conformations. Further insight can be obtained by comparing the results presented herein with previous studies. We start out with a comparison of the free

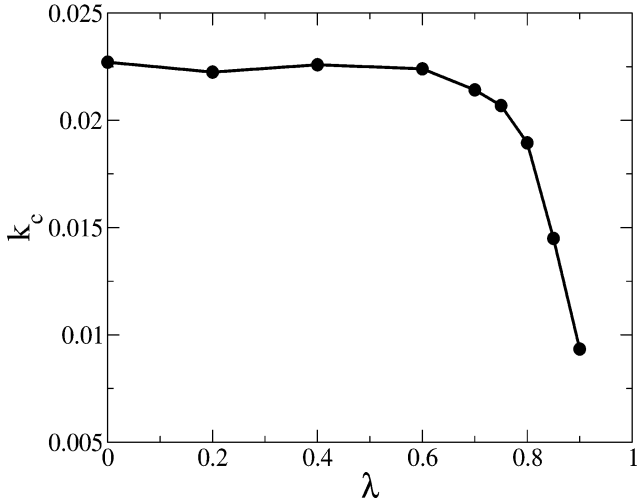

Figure 11. The dependence of the average collapse rate on the surface "attractiveness", as measured by the value of λ. The prohibitively small value of k_c for $\lambda = 1.0$ could not be calculated with reasonable statistics on the basis of our simulations.

polymer results presented above, which were obtained for a homopolymer model, with the results presented in ref 36, which were obtained for a free 22-mer heteropolymer model of a protein. The end-to-end distance distribution for the homopolymer in the coiled state is qualitatively similar to that of the unfolded protein. However, a closer inspection reveals that, while the distribution is symmetrical in the case of the homopolymer, it is significantly asymmetrical in the case of the protein model, which can be attributed to a residual structure that characterizes the protein in its unfolded state. Furthermore, the end-to-end distance distribution for the homopolymer in the globular state is qualitatively different from that of the folded protein. More specifically, while the homopolymer adopts liquid-droplet-like conformations in the globular state, the protein model is designed to give rise to a well-defined and relatively rigid structure in the native state. As a result, the distribution of the end-to-end distance is unimodal in the case of the folded protein, while being multimodal in the case of the homopolymer.

Similarly, the potential of mean force corresponds to a single deep well around the native state in the protein case, while being very ragged, with a multitude of local minima, in the case of the homopolymer.

The difference between the homopolymer and the protein models also manifests itself in the dynamics. In the case of the protein model, the native state is characterized by rapid dynamics that stretches on a relatively narrow window of time scales (in comparison to the unfolded state). On the other hand, the decay of the end-to-end distance correlation function in the homopolymer case reflects fast intrashell dynamics as well as slow intershell dynamics and therefore stretches over a range of time scales that are in fact wider than in the coiled state. However, despite those opposite trends, $\bar{D}(\langle R \rangle T_W)$ is smaller, on average, in the globular/folded state than in the coiled/unfolded state. This is self-evident in the protein case, since motion in the folded state occurs on faster time scales and therefore reaches the ergodic limit more quickly. The fact that the same trend is also observed in the case of the homopolymer rejects the fact that $\bar{D}(\langle R \rangle T_W)$ is dominated by the fast intrashell motion, rather than by the relatively infrequent intershell barrier-crossing events. The polymer collapse via a two-step process, starting with the formation of local blobs separated by linear segments which later coalesce into a globule, was previously reported and discussed by Chang and Yethiraj.[52] The authors of ref 52 have found that this pathway dominates when Brownian dynamics were employed in order to simulate the collapse dynamics of a homopolymer model which is very similar to the one employed here. This should be contrasted with our observation that collapse via a single-step pathway is even more common, particularly when the initial coiled conformation is characterized by a short end-to-end distance (cf. section III. D). This discrepancy can be explained by the sensitivity of the results to the quenching depth, ϵ/k_BT. More specifically, the two-step pathway may indeed be dominant at large quench depths ($\epsilon/k_BT > 5$) but becomes less important at smaller quench depths (e.g., at $\epsilon/k_BT = 2.5$, as in our case). Interestingly, the authors of ref 52 have also argued that the two-step pathway is not observed when an explicit solvent is employed. However, we have found similar contributions from the one-step and two-step pathways, regardless of whether the solvent is treated explicitly (not shown), which can probably also be attributed to the small quenching depth employed here. Finally, we note that other important new aspects considered here, which to the best of our knowledge were not considered in previous studies, include the effect of surface immobilization on the end-to-end distance distributions as well as the correlation between the initial conformation and the rate and pathway of collapse. It should be noted that the FRET efficiency distributions obtained from actual experiments also reflect fluctuations due to sources other than polymer conformational dynamics, including shot noise, spectral diffusion, and dipole angle distributions. Those other sources of noise were not accounted for in the simulations reported in this paper. Nevertheless, we hope that our results will provide guidance for the interpretation of single-molecule FRET experiments performed on surface-immobilized and free polymers. Other aspects regarding polymer dynamics which are particularly relevant to single-molecule experiments can be explored within the theoretical and computational framework employed here, for example: (1) How will the predictions change if the polymer model includes bending and torsion potentials, heterogeneity along the backbone, and branching? (2) What will be the impact of long-range (e.g., electrostatic) interactions with the surface? (3) Can the globular conformations be controlled via the surface geometry? Those questions and others will be the subject of future research.

Acknowledgment. The authors are grateful to Dr. Dong Wang for helpful discussions and to the Petroleum Research Fund for financial support (through grant no. 36486-G).

References and Notes

(1) de Gennes, P. G. *Scaling concepts in polymer physics*; Cornell University Press: Ithaca, NY, 1979.

(2) Doi, M.; Edwards, S. F. *The theory of polymer dynamics*; Clarendon Press: Oxford, 1986.

(3) Edman, L.; Mets, Ü.; Rigler, R. *Proc. Natl. Acad. Sci. U.S.A.* **1996**, *93*, 6710.

(4) Nie, S.; Zare, R. N. *Annu. Rev. Biophys. Struct.* **1997**, *26*, 567.

(5) Jia, Y.; Sytnik, A.; Li, L.; Vladimirov, S.; Cooperman, B. S.; Hochstrasser, R. M. *Proc. Natl. Acad. Sci. U.S.A.* **1997**, *94*, 7932.

(6) Xi, X. S.; Trautman, J. K. *Ann. Rev. Phys. Chem.* **1998**, *49*, 441.

(7) Weiss, S. *Science* **1999**, *283*, 1676.

(8) Ha, T.; Ting, A. Y.; Liang, J.; Caldwell, D. B.; Denize, A. A.; Chemla, D. S.; Schultz, P. G.; Weiss, S. *Proc. Natl. Acad. Sci. U.S.A.* **1999**, *96*, 893.

(9) Ha, T.; Zhuang, X.; Kim, H. D.; Orr, J. W.; Williamson, J. R.; Chu, S. *Proc. Natl. Acad. Sci. U.S.A.* **1999**, *96*, 9077.

(10) Geva, E.; Skinner, J. L. *Chem. Phys. Lett.* **1998**, *288*, 225.

(11) Jia, Y.; Talaga, D. S.; Lau, W. L.; Lu, H. S. M.; DeGrado, W. F.; Hochstrasser, R. M. *Chem. Phys.* **1999**, *247*, 69.

(12) Hu, D.; Yu, J.; Wong, K.; Bagchi, B.; Rossky, P.; Barabara, P. F. *Nature (London)* **2000**, *405*, 1030.

(13) Russel, R.; Zhuang, X. W.; Babcock, H. P.; Millet, I. S.; Doniach, S.; Chu, S.; Herschlag, D. *Proc. Natl. Acad. Sci. U.S.A.* **2002**, *99*, 155.
(14) Bartley, L. E.; Zhuang, X. W.; Das, R.; Chu, S.; Herschlag, D. J. *Mol. Biol.* **2003**, *6*, 923.
(15) Zhuang, X. W.; Reif, M. *Curr. Opin. Struct. Biol.* **2003**, *13*, 88.
(16) Chu, S. *Phil. Trans. R. Soc. London, Ser. A* **2003**, *361*, 689.
(17) Kubelka, J.; Hofrichter, J.; Eaton, W. A. *Curr. Opin. Struct. Biol.* **2004**, *14*, 76.
(18) Fernandez, J. M.; Li, H. *Chem. Phys.* **2004**, *303*, 1674.
(19) Ha, T.; Enderle, T.; Oglertee, D. F.; Chemla, D. S.; Selvin, P. R.; Weiss, S. *Proc. Natl. Acad. Sci. U.S.A.* **1996**, *93*, 6264.
(20) Ha, T.; Ting, A. Y.; Liang, J.; Denize, A. A.; Chemla, D. S.; Schultz, P. G.; Weiss, S. *Chem. Phys.* **1999**, *247*, 107.
(21) Deniz, A. A.; Dahan, M.; Grunwell, J. R.; Ha, T.; Faulhaber, A. E.; Chemla, D. S.; Weiss, S.; Schultz, P. G. *Proc. Natl. Acad. Sci. U.S.A.* **1999**, *96*, 3670.
(22) Ishii, Y.; Yoshida, T.; Funatsu, T.; Wazawa, T.; Yanagida, T. *Chem. Phys.* **1999**, *247*, 163.
(23) Talaga, D. S.; Lau, W. L.; Roder, H.; Tang, J.; Jia, Y.; DeGrado, W. F.; Hochstrasser, R. M. *Proc. Natl. Acad. Sci. U.S.A.* **2000**, *97*, 13021.
(24) Deniz, A. A.; Laurence, T. A.; Beligere, G. S.; Dahan, M.; Martin, A. B.; Chemla, D. S.; Dawson, P. E.; Schultz, P. G.; Weiss, S. *Proc. Natl. Acad. Sci. U.S.A.* **2000**, *97*, 5179.
(25) Weiss, S. *Nat. Struct. Biol.* **2000**, *7*, 724.
(26) Ying, L.; Wallace, M. L.; Balasubramainian, S.; Klenerman, D. *J. Phys. Chem. B* **2000**, *104*, 5171.
(27) Brasselet, S.; Peterman, E. J. G.; Miyawaki, A.; Moerner, W. E. *J. Phys. Chem. B* **2000**, *104*, 3676.
(28) Zhuang, X.; Kim, H.; Pereira, M. J.; Babcock, H. P.; Walter, N. G.; Chu, S. *Science* **2002**, *296*, 1473.
(29) Schuler, B.; Lipman, E. A.; Eaton, W. A. *Nature (London)* **2002**, *419*, 743.
(30) Lipman, E. A.; Schuler, B.; Bakajin, O.; Eaton, W. A. *Science* **2003**, *301*, 1233.
(31) Haran, G. J. *Phys.: Condens. Matter* **2003**, *15*, R1291.
(32) Rhoades, E.; Gussakovsky, E.; Haran, G. *Proc. Natl. Acad. Sci. U.S.A.* **2003**, *100*, 3197.
(33) Rhoades, E.; Cohen, M.; Schuler, B.; Haran, G. *J. Am. Chem. Soc.* **2004**, *126*, 14686.
(34) Yang, H.; Witkoskie, J. B.; Cao, J. S. *J. Chem. Phys.* **2002**, *117*, 11010.
(35) Gopich, I. V.; Szabo, A. *J. Phys. Chem. B* **2003**, *107*, 5058.
(36) Wang, D.; Geva, E. *J. Phys. Chem. B* **2005**, *109*, 1626.
(37) Srinivas, G.; Bagchi, B. *Chem. Phys. Lett.* **2000**, *328*, 420.
(38) Srinivas, G.; Yethiraj, A.; Bagchi, B. *J. Phys. Chem. B* **2001**, *105*, 2475.
(39) Srinivas, G.; Yethiraj, A.; Bagchi, B. *J. Chem. Phys.* **2001**, *114*, 9170.
(40) Srinivas, G.; Bagchi, B. *J. Chem. Phys.* **2002**, *116*, 837.
(41) Srinivas, G.; Bagchi, B. *Phys. Chem. Comm.* **2002**, *5*, 59.
(42) Stryer, L.; Haugland, R. P. *Proc. Natl. Acad. Sci. U.S.A.* **1967**, *58*, 719.
(43) Haas, E.; Wilchek, M.; Katchalski-Katzir, E.; Steinberg, I. Z. *Proc. Natl. Acad. Sci. U.S.A.* **1975**, *72*, 1807.
(44) Selvin, P. R. *Methods Enzymol.* **1995**, *246*, 300.
(45) Andrews, D. L.; Demidov, A. A. *Resonance energy transfer*; Wiley: New York, 1999.
(46) Selvin, P. R. *Nat. Struct. Biol.* **2000**, *7*, 730.
(47) Förster, T. *Ann. Phys. (Leipzig)* **1948**, *2*, 55.
(48) Dexter, D. L. *J. Chem. Phys.* **1953**, *21* (5), 836.
(49) Scholes, G. D. *Annu. Rev. Phys. Chem.* **2003**, *54*, 57.
(50) Honeycutt, J. D.; Thirumalai, D. *Biopolymers* **1992**, *32*, 695.
(51) Veithans, T.; Klimov, D.; Thirumalai, D. *Folding Des.* **1996**, *2*, 1.
(52) Chang, R.; Yethiraj, A. *J. Chem. Phys.* **2001**, *114*, 7688.